

EXPERIMENTAL STUDY ON MODE-I DELAMINATION OF THERMOPLASTIC COMPOSITES USING DIGITAL IMAGE CORRELATION AND ACOUSTIC EMISSION

Javane Karami^{1*}, Kalliopi-Artemi Kalteremidou¹, Dimitrios Aggelis¹ and Danny Van Hemelrijck¹

¹ Mechanics of Materials and Constructions (MeMC), Vrije Universiteit Brussel (VUB), Brussels, Belgium

* Corresponding author (Javane.karami@vub.be)

Keywords: Delamination, Mode I fracture, DCB test, Acoustic emission, Thermoplastics

ABSTRACT

The mode I delamination of a unidirectional thermoplastic composite is investigated in this work by applying Non-Destructive Techniques (NDT) like 3D Digital Image Correlation (DIC) and Acoustic Emission (AE). Using the AE data, wave features are extracted. To calculate the fracture toughness, the crack length is measured using the DIC technique and the three data reduction methods provided by ASTM D5528 are applied. All the methods resulted in the same fracture toughness values for initiation and propagation of the crack. The results of this preliminary study will be used in the future to be compared with the results of mode II delamination tests and in turn, as a basis to better understand the delamination behaviour of the considered composite material under mixed mode I/II loading.

1 INTRODUCTION

Design flexibility, great mechanical properties, and high strength to weight ratio [1] have widened the application of laminated composites in various industries like aerospace, automotive and wind turbines. Based on the loading and environmental conditions, composites experience different damage mechanisms like matrix cracking, fiber pull-out, fiber-matrix debonding, fiber breakage, and delamination [2]. Among these, delamination is considered one of the most detrimental damage modes in polymer composites [1]. During their service life, composites may experience delamination under a combination of opening (mode I) and shearing modes (mode II and mode III). Therefore, understanding the delamination behaviour of composites under mixed mode loading is crucial since it can lead to more reliable design of composite structures, therefore alleviating the need for high safety factors [1]. However, before conducting mixed mode experiments, pure mode tests (like pure mode I and II) have to be assessed.

Many studies in literature have used Non-Destructive Techniques (NDT) to monitor different damage mechanisms together with the corresponding damage sequences. The experimental examination of the delamination behaviour of composites using NDT has also been a topic of interest for researchers on the field. For instance, the Acoustic Emission (AE) technique has been successfully applied in many delamination tests to detect the onset of crack initiation [2], to localize the crack front during loading [3] or to classify the damage mechanisms [2], [4, 5] to name a few. Most of these studies deal with the mode I delamination while there are fewer studies [6, 7] on the mode II and mixed mode I/II delaminations in composites using the AE technique.

Accordingly, the AE method in combination with the Digital Image Correlation (DIC) technique is utilized in the current study to conduct mode I delamination tests. The crack was monitored using the DIC technique while the AE system was capturing the elastic waves that were generated as a result of the different damage mechanisms taking place in the composite. The test results are divided in two parts; in the first part, the preliminary AE analyses are provided while the second part deals with the calculation of the fracture toughness. The results of this study will be used in the future to be compared with the results of mode II delamination tests and as a basis to better understand the delamination behaviour under mixed mode I/II loading.

2 SPECIMEN PREPARATION AND TEST SET-UP

Double Cantilever Beam (DCB) test specimens were made out of a thermoplastic composite reinforced with unidirectional carbon fibers. To create the pre-crack, Kapton film (containing release agent) was placed in the composite mid-section before consolidation. The composite plate was cut using a diamond saw; the dimensions (4.4*25*230 mm, pre-crack length of 50 mm, based on ASTM D5528 [8]) together with the position of the Pico sensors for AE measurements are depicted in Fig. 1. One sensor was located above the crack front while the other one was located 50 mm away. The Pico sensors are relatively broadband with a peak sensitivity at 450 kHz.

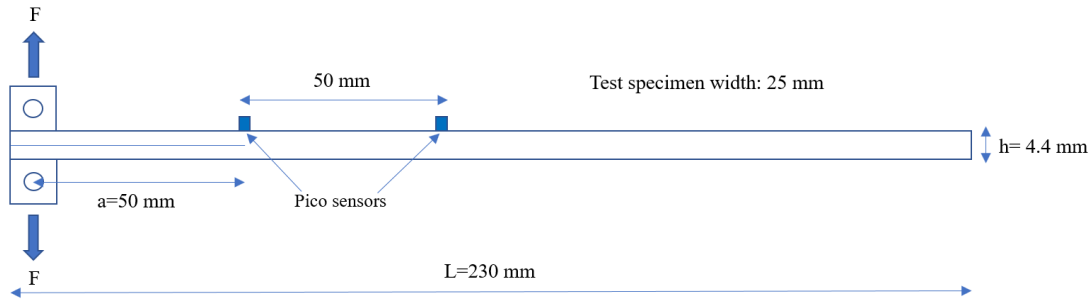


Fig. 1. DCB test specimen dimensions and positions of the Pico sensors

Aluminum loading blocks were attached to the specimens and tensile loading was applied using an Instron universal testing machine. Initially, to create a natural pre-crack and to remove the resin pocket, the specimens were loaded with a displacement rate of 2 mm/min. When reaching a crack growth length of approximately 5 mm (as suggested by ASTM D5528), the specimens were unloaded with a displacement rate of 25 mm/min. Then, a displacement rate of 2 mm/min was applied. The load was recorded by the testing machine while the displacement and the crack length were monitored by a stereo DIC system.

Regarding the DIC set-up, a layer of white paint was applied on the specimen edge, being as thin as possible to avoid uncertainties in the measurement of the crack length. Moreover, the applied black speckle pattern was as fine as possible so that small enough subsets could be used to capture the local deformations arising from crack initiation and propagation. The subset size was set to 15 pixels while the step size was almost one fourth of the subset size (4 pixels), as suggested by [9]. It is worth to mention that the total displacement measured by the 3D DIC system, and the loading machine were almost identical, and that the DIC analyses were mostly useful in indicating the position of the crack front by using the sigma parameter (in pixels) (Fig. 2).

The sigma parameter shows the confidence interval between the deformed and the reference image. When it equals to zero it shows a perfect correlation between the two, while a higher value represents weaker correlations and in turn, less reliable results for an unloaded specimen [10]. Considering a cracked specimen, when the crack initiates, the displacement field around the crack tip becomes non-continuous, causing higher errors in correlation or higher values of sigma [10]. Accordingly, as suggested in [11] the position of the crack front can be indicated by defining a sigma threshold value that is higher than the noise level of the DIC analyses. In this study, the noise level was measured by taking images from the specimen before applying the mechanical loads. Then, an average value of 0.016 pixels was chosen as the sigma threshold to identify the position of the crack front.

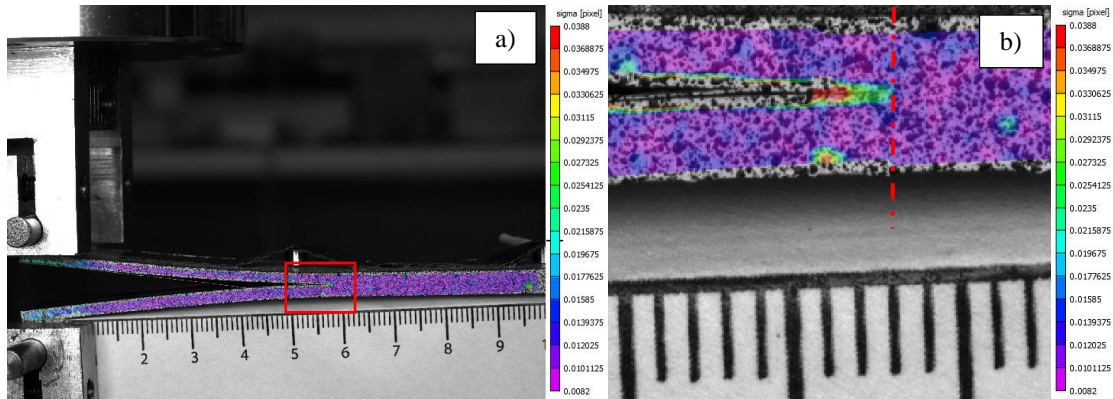


Fig. 2. a) Distribution of the sigma parameter on the surface of the test specimen, b) magnified view around the crack front

3 DCB EXPERIMENTS

3.1 Acoustic emission analyses

A total number of 5 specimens were tested, among which, the variations in load and acoustic emission energy for one specimen are shown in Fig. 3(a). In this specimen, the initiation of the crack was visually observed (using the DIC system) at a point that was almost identical to the maximum load. Accordingly, a dashed line passing through this point was added in the graph to better distinguish the AE activities that were recorded before and after crack initiation. As it can be seen, the released AE energy before this point is negligible in comparison to the overall process. Furthermore, an increase in the acoustic energy is taking place before crack initiation (the point of maximum load, Fig. 3(a)).

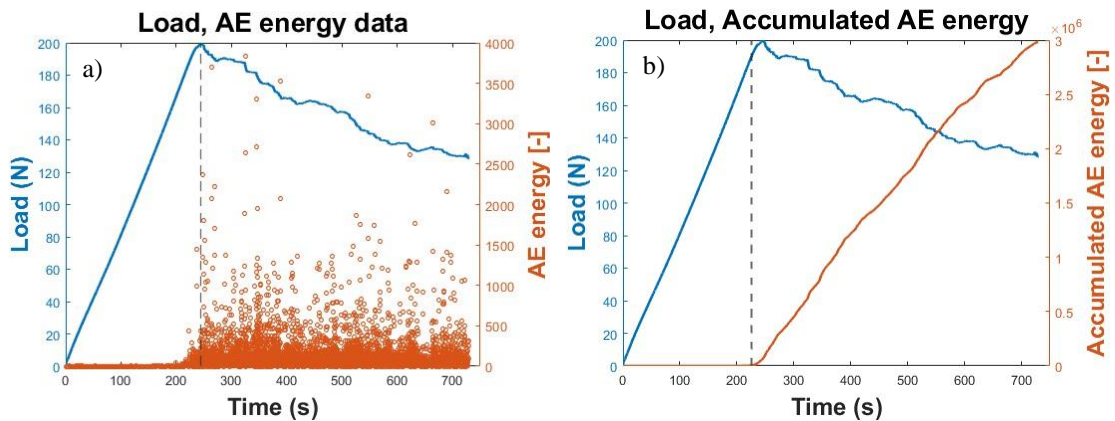


Fig. 3. a) Load and AE energy data versus time, b) load and accumulated acoustic emission energy

In order to identify the point at which the crack initiates, three different methods are provided by ASTM D5528; 1- the beginning of non-linearity in the load-displacement curve, 2- the point at which crack initiation can be visually observed by an optical microscope with a maximum magnification of 70x, and 3- the intersection of the load-displacement curve with a straight line starting from the origin and having a slope of 1.05 times the compliance of the linear portion. The point of maximum load would be considered instead in case that the intersection occurs after the maximum load.

Furthermore, other ways of identifying the crack initiation moment based on the AE technique are provided in literatures. For instance, the first significant rise in the cumulative curve of AE energy (the

integral of the rectified signal envelope), counts or number of events, the first instant drop in the Sentry function (a parameter combining the mechanical and the AE energy) [2] or the first considerable increase in the RA value (rise time divided by amplitude) [12] can be mentioned. However, it should be noted that these methods are qualitative [2] and hence, may not be always accurate. For more detailed information about the drawbacks of the qualitative AE methods in identifying damage initiation in composite materials, readers are referred to [2].

In this study, the fracture toughness is calculated based on the moment of crack initiation that is visually observed by the DIC system.

In Fig. 3(b), the load-time curve together with the accumulated AE energy is depicted. In this figure, the dashed line represents the moment at which we observe a considerable increase in the cumulative AE energy. This point is located before the moment the crack visually initiates (maximum load in Fig. 1) and corresponds to 95% of the maximum load. This may be due to the occurrence of low intensity micro damages that are being recorded by the AE system before they lead to a considerable load drop [2].

In the next step, the AE data were grouped in three different classes in order to extract the waveform features and to check their variations among the different groups. In Fig. 4, the three different classes are depicted. The first class corresponds to the start of loading till the point where an increase is observed in the cumulative acoustic emission energy. Then, the second class starts from the end of the first class and continues till the maximum load. As for the third class, it includes all the data points from the maximum load onwards. Before analyzing the AE wave features for the DCB specimens, all parameters are defined in Fig. 5.

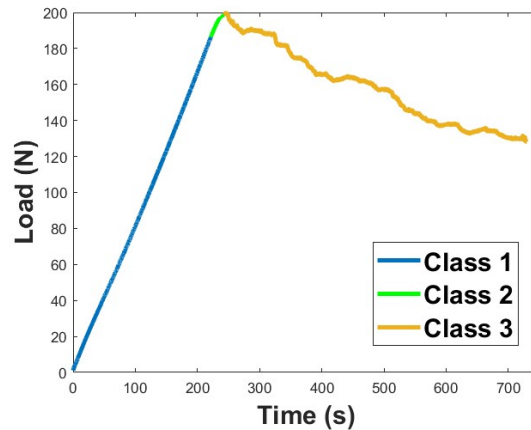


Fig. 4. Defining three different classes for AE analyses based on the Load-time data points

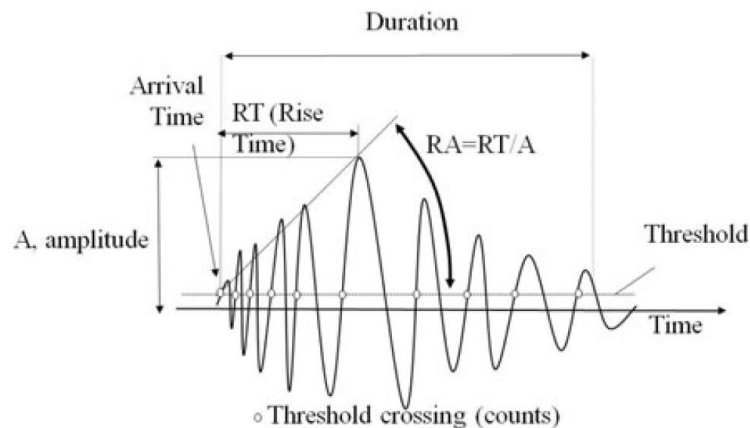


Fig. 5. Definition of the acoustic waveform parameters [13]

In Table 1, the average values of the AE wave features are provided, in which, ‘En.’, ‘AF’ and ‘RT’ stand for energy, average frequency (number of counts divided by duration) and rise time, respectively. As depicted in Fig. 5, RA is defined by the ratio between the rise time and amplitude. The numbers (1, 2 and 3) following the features are standing for the class number (test stage) from which these parameters were extracted. Considering the results provided in Table 1, two conclusions can be drawn:

- 1- As the loading increases (moving from class 1 to class 3), the average values of the AE energy increase as well. This is due to the fact that at the initial stages of loading (especially in the linear portion of the load-displacement curve) matrix micro-cracking is taking place, releasing low AE energy quantities. However, as the load increases, the micro-cracks increase and other damage mechanisms like delamination, fiber-matrix debonding, fiber bridging and fiber fracture are taking place which in turn release more and more AE energy. Other parameters like RT, RA and duration (not provided in the table) also increase, which shows a potential shift towards shear-related activities [13] that may be associated with damage mechanisms like fiber-matrix debonding. On the other hand, a decrease in the average frequency can be observed, which is again an indication of shear mode micro-cracks [13].
- 2- Considering each class, the average values among different specimens are quite repeatable. This fact shows the quality and reproducibility of the applied manufacturing process as well as the designed test set-up. This is due to the fact that manufacturing techniques play a vital role in creating initial imperfections like matrix cracks, fiber misalignment, voids in the fibers and matrix and inclusion of impurities to name a few [14], with some of them causing a considerable release of AE energy [2]. This reproducible behavior allows for the establishment of an “acoustic signature” for the mode I cracking events, which seem to be characterized by approximately 250 kHz average frequency and 7 μ s RT at the onset of the loading activity. Establishing this signature will enable comparison with the mode II and mixed mode experiments that will follow.

Table 1. AE waveform features extracted for different classes and specimens

	<i>En.1 [-]</i>	<i>En.2 [-]</i>	<i>En.3 [-]</i>	<i>AF1 [kHz]</i>	<i>AF2 [kHz]</i>	<i>AF3 [kHz]</i>
<i>S1</i>	0.40	9.53	7.50	237.64	205.83	205.15
<i>S2</i>	0.88	7.52	9.90	242.14	208.73	190.98
<i>S3</i>	0.28	7.78	7.64	243.37	221.97	199.59
<i>S4</i>	0.25	8.57	9.18	276.76	206.58	193.47
<i>S5</i>	0.45	7.79	9.67	280.54	193.75	180.80
Avg.	0.45	8.24	8.78	256.09	207.37	194.00
C.O.V. (%)	50.278	8.925	11.547	7.25	4.33	4.25
	<i>RT1 [μs]</i>	<i>RT2 [μs]</i>	<i>RT3 [μs]</i>	<i>RA1 [μs/dB]</i>	<i>RA2 [μs/dB]</i>	<i>RA3 [μs/dB]</i>
<i>S1</i>	8.01	19.902	21.15	0.18	0.36	0.39
<i>S2</i>	8.71	20.02	22.27	0.19	0.38	0.41
<i>S3</i>	7.42	18.19	22.17	0.17	0.34	0.41
<i>S4</i>	6.00	18.99	22.02	0.14	0.35	0.40
<i>S5</i>	6.03	20.01	23.00	0.14	0.37	0.42
Avg.	7.23	19.42	22.14	0.16	0.36	0.41
C.O.V. (%)	14.88	3.72	2.70	14.15	3.44	2.83

Finally, to check the correlation between the DIC driven and AE driven data, the crack length at random moments was measured using the DIC system, and the corresponding cumulative AE energy was extracted at those moments as seen in Fig. 6. In Fig. 6(a), a strong linear relation between the crack length and the cumulative AE energy can be observed, being in line with previous studies like [3]. However, in the same study it is mentioned that using a linear relation between the mentioned parameters will overestimate the crack length for the initiation values due to the dominance of matrix cracking that produces low energy in comparison to the other damage mechanisms that are being involved in the delamination process. Accordingly, in [4] a 3rd degree polynomial fitting was suggested to address this problem. In Fig. 6, by comparing the linear and the polynomial fitting it is seen that for the latter one the norm of the residuals is less. Therefore, the observed results show the correlation between the AE and DIC data and indicate that either technique could be used to track the crack behavior.

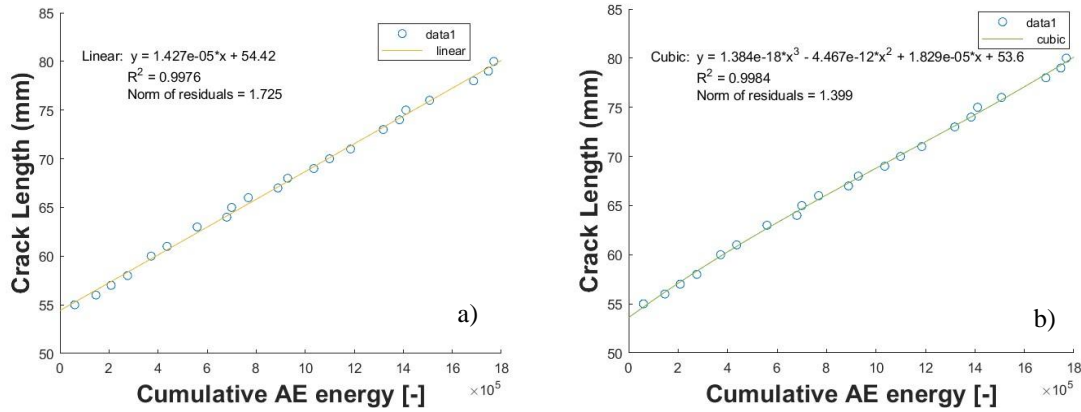


Fig. 6. a) Linear and b) 3rd degree polynomial regression of crack length-cumulative AE energy

3.2 Fracture toughness calculation

Based on ASTM D5528, three different ways of calculating the critical energy release rate or the fracture toughness are provided; 1- the Modified Beam Theory (MBT), 2- the Compliance Calibration method (CC) and 3- the Modified Compliance Calibration method (MCC). The formula for these three different methods is provided by equations 1-3, respectively.

$$G_{Ic} = \frac{3P\delta}{2b(a + |\Delta|)} \quad (1)$$

where G_{Ic} , P , δ , b and a stand for the fracture toughness, load, displacement, average width of the specimen and the crack length, respectively. As for Δ , it is the root of the curve $(C^{1/3}-a)$ in which C is the compliance of the test specimen. For the CC method:

$$G_{Ic} = \frac{nP\delta}{2ba} \quad (2)$$

In this method, n is calculated by measuring the slope of the $(\log(C)-\log(a))$ graph. Finally, for the modified compliance calibration method the following equation applies:

$$G_{Ic} = \frac{3P^2C^{2/3}}{2A_1bh} \quad (3)$$

where h stands for the overall thickness of the DCB specimen and A_1 is the slope of the $(a/h-C^{1/3})$ graph. Based on the provided equations, it is necessary to measure the load, displacement, and the crack length during loading. As already mentioned, the load was measured using the tensile machine while the rest were monitored by using the 3D DIC system. Based on the acquired data, the initiation values for the fracture toughness based on the modified beam theory method and the point where initiation is observed visually by the DIC system are given in Table 2.

Table 2. Fracture toughness initiation values based on the modified beam theory

Specimen	G_{Ic} [kJ/m ²]
1	1.75
2	1.65
3	1.68
4	1.57
5	1.41
Avg.	1.61
SD	0.12

For all the specimens, the fracture toughness was calculated both for the initiation moment as well as for the propagation of the crack using the three different methods provided by ASTM D5528. It is worth to mention that the differences between the results of the applied data reduction methods were negligible (Fig. 7). In Fig. 7, the first data point corresponds to the moment that the crack starts to grow (visually) from the insert, and since in this stage the crack passes through a resin pocket, the calculated energy release rate is very low in comparison to the other data points. The points 2 and 3 were calculated based on the pre-cracking loading stage of the DCB specimen, and the 4th data point corresponds to the visual initiation value in the pre-cracked specimen.

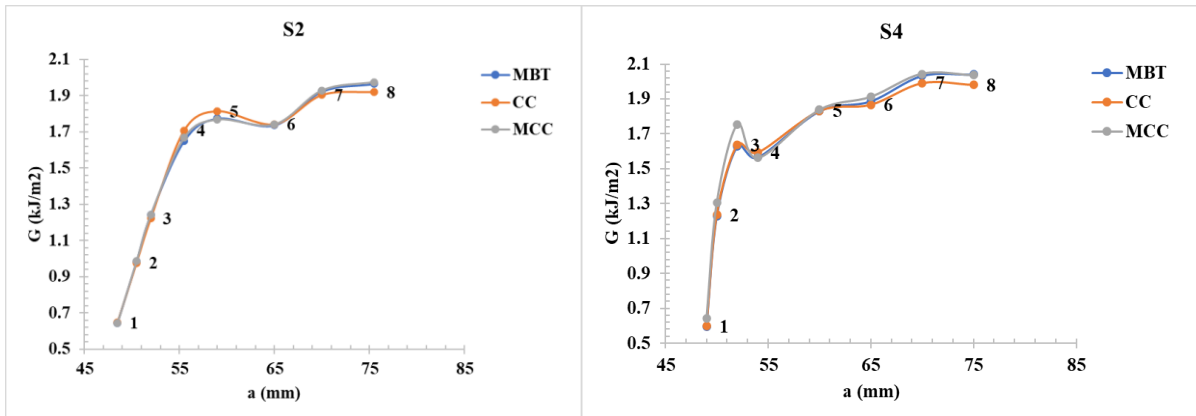


Fig. 7. The resistance curve (R-curve) for two different specimens based on three different data reduction methods

4 SUMMARY AND CONCLUSIONS

The mode I delamination of a unidirectional thermoplastic composite was investigated using non-destructive techniques like 3D DIC and AE. The AE wave features were extracted for all the test specimens and compared with each other. The low differences of the average AE wave feature values between the specimens showed the reproducibility of the applied manufacturing method as well as of the experimental test set-up. Furthermore, the extracted 3rd degree polynomial relation between the

accumulated AE energy and the crack length was not only in line with the previous studies but was also an indication of the correlation between the data extracted using the AE and the DIC methods. To calculate the fracture toughness, the three different data reduction methods provided by ASTM D5528 were applied and all of them resulted in almost the same fracture toughness values for initiation and propagation of the crack. The results of this preliminary study will be compared with mode II delamination tests and will be used as a basis to better understand the delamination behavior of the applied composite material under mixed mode I/II loading.

ACKNOWLEDGEMENTS

The authors would like to thank Innoviris for funding the project “Stamping of thermoplastic composite materials”.

REFERENCES

- [1] P. K. Asur Vijaya Kumar, A. Dean, J. Reinoso, and M. Paggi, “A multi phase-field-cohesive zone model for laminated composites: Application to delamination migration,” *Compos Struct*, vol. 276, Nov. 2021, doi: 10.1016/j.compstruct.2021.114471.
- [2] M. Saeedifar and D. Zarouchas, “Damage characterization of laminated composites using acoustic emission: A review,” *Composites Part B: Engineering*, vol. 195. Elsevier Ltd, Aug. 15, 2020. doi: 10.1016/j.compositesb.2020.108039.
- [3] M. Fotouhi, M. Saeedifar, J. Yousefi, and S. Fotouhi, “The application of Acoustic Emission technique in the delamination of laminated composites,” in *Focus on Acoustic Emission Research*, C. Barlie and G. Pappalettera, Eds., NOVA Publishers, 2017. Accessed: May 18, 2023. [Online]. Available: <https://research-information.bris.ac.uk/en/publications/the-application-of-an-acoustic-emission-technique-in-the-delamina>
- [4] M. Saeedifar, M. Ahmadi Najafabadi, K. Mohammadi, M. Fotouhi, H. Hosseini Toudeshky, and R. Mohammadi, “Acoustic Emission-Based Methodology to Evaluate Delamination Crack Growth Under Quasi-static and Fatigue Loading Conditions,” *J Nondestr Eval*, vol. 37, no. 1, Mar. 2018, doi: 10.1007/s10921-017-0454-0.
- [5] S. Samborski, A. Gliszczynski, J. Rzeczkowski, and N. Wiacek, “Mode I interlaminar fracture of glass/epoxy unidirectional laminates. Part I: Experimental studies,” *Materials*, vol. 12, no. 10, May 2019, doi: 10.3390/ma12101607.
- [6] M. Saeedifar, M. Fotouhi, M. A. Najafabadi, and H. H. Toudeshky, “Interlaminar Fracture Toughness Evaluation in Glass/Epoxy Composites Using Acoustic Emission and Finite Element Methods,” *J Mater Eng Perform*, vol. 24, no. 1, pp. 373–384, Jan. 2015, doi: 10.1007/s11665-014-1291-2.
- [7] S. Goutianos, “Acoustic emission characteristics of unidirectional glass/epoxy composites under mixed-mode fracture,” *SN Appl Sci*, vol. 1, no. 5, May 2019, doi: 10.1007/s42452-019-0499-z.
- [8] ASTM, “Standard Test Method for Mode I Interlaminar Fracture Toughness of Unidirectional Fiber-Reinforced Polymer Matrix Composites 1,” 2007. [Online]. Available: www.astm.org,
- [9] N. 'Lovaas, “Subset, Step Size and Strain Filter Selection,” *Correlated Solutions, Inc.*, 2021. <https://correlated.kayako.com/article/44-subset-step-size-and-strain-filter-selection> (accessed May 03, 2023).
- [10] M. Zhu and S. V Lomov Larissa Gorbatiikh, “Modeling and characterization of fatigue delamination in unidirectional laminates,” 2019. Accessed: May 18, 2023. [Online]. Available: https://kuleuven.limo.libis.be/discovery/search?query=any,contains,LIRIAS2812209&tab=LIRIAS&search_scope=lirias_profile&vid=32KUL_KUL:Lirias&offset=0
- [11] B. R. Murray *et al.*, “Crack Tip Monitoring of Mode I and Mode II Delamination in CF/Epoxy under Static and Dynamic Loading Conditions Using Digital Image Correlation,” MDPI AG, May 2018, p. 389. doi: 10.3390/icem18-05225.
- [12] W. Li, Y. Liu, P. Jiang, F. Guo, and J. Cheng, “Study on Delamination Damage of CFRP Laminates Based on Acoustic Emission and Micro Visualization,” *Materials*, vol. 15, no. 4, Feb. 2022, doi: 10.3390/ma15041483.

- [13] D. G. Aggelis and T. Shiotani, "Parameters Based AE Analysis," in *Acoustic Emission Testing, Basics for Research - Applications in Engineering*, 2nd ed. Springer Cham, pp. 45–72. doi: <https://doi.org/10.1007/978-3-030-67936-1>.
- [14] O. E. Suleiman Khayal, "Literature review on imperfection of composite laminated plates," *J Microsc Ultrastruct*, vol. 5, no. 3, p. 119, 2017, doi: 10.1016/j.jmau.2017.01.001.